Available online at www.sciencedirect.com

SciVerse ScienceDirect

Ceramics International 38 (2012) 3281–3290

CERAMICS INTERNATIONAL

www.elsevier.com/locate/ceramint

The effects of SiO_2 and K_2O on glass forming ability and structure of $CaO–TiO_2–P_2O_5$ glass system

H.R. Ahmadi Mooghari [a,*], Ali Nemati [b], B. Eftekhari Yekta [c], Z. Hamnabard [d]

[a] Department of Materials Engineering, Science and Research Branch, Islamic Azad University, Tehran, Iran
[b] Department of Materials Science and Engineering, Sharif University of Technology, Tehran, Iran
[c] Ceramic Division, Department of Metallurgy and Materials Engineering, Iran University of Science & Technology, Narmak, Tehran, Iran
[d] Ceramic Group, Materials Research School, P.O. Box 14395-836, Karaj, Alborz, Iran

Received 13 August 2011; received in revised form 28 November 2011; accepted 13 December 2011
Available online 29 December 2011

Abstract

The effects of SiO_2 and K_2O were investigated on the glass forming ability (GFA) and structural characteristics of $CaO–TiO_2–P_2O_5$ system. Differential thermal analyzer (DTA), X-ray diffraction (XRD), scanning electron microscopy (SEM), FT-IR and ^{31}P magic angle spinning NMR methods were applied for characterizations of the system.

Unwanted crystallization in the initial three components base glass composition was observed by adding SiO_2 and crystalline phases such as TiP_2O_7, rutile (TiO_2) and cristobalite (SiO_2) were formed in it.

The results showed that K_2O prevents crystallization of glasses and promotes the formation of glass. FT-IR and X-ray diffraction showed that the addition of K_2O caused the formation of phosphate–silicate network as P–O–Si, and formation of isolated droplet phases (rich of Si and P) separated from the phosphate matrix.

The optimum amounts of SiO_2 and K_2O in phosphate structure were respectively 6 and 2 wt.%, 0 in accordance with glass forming ability (GFA) parameters. Despite addition of SiO_2 along with K_2O; the ^{31}P MAS NMR and infrared spectrums of glasses show that no Q^2 sites were in the phosphate network. The Q^1 and the pyrophosphate groups was the predominant structural unit in these glasses.
© 2011 Elsevier Ltd and Techna Group S.r.l. All rights reserved.

Keywords: DTA; FT-IR; NMR; Glass forming ability

1. Introduction

Phosphate glasses have recently been considered for many applications due to a series of attractive properties such as low glass transition and melting temperatures, high thermal expansion coefficient, biocompatibility, low dispersion and high refractive indices, which recommend them in many applications such as, photonics, fast ion conductors [1–4], glass to metal seals [5,6], self-cleaning ability for NH_3 gas adsorption [7], and most recently biomedical engineering [8]. The studied have clarified that these applications require the optimization of phosphate-based glasses property that is achievable by tuning their composition and structure.

The glass forming regions in the $CaO–TiO_2–P_2O_5$ system was investigated by Akira Kishioka [9]. He has claimed glass-forming in this system is fundamentally limited [10]. In 1989, Hosono et al. introduced a new phosphate based glass–ceramic in the $CaO–TiO_2–P_2O_5$ system which composed of β-$Ca_3(PO_4)_2$ and $CaTi_4(PO_4)_6$ phases [10]. In 1990s, they adjusted the glass system ($CaO–TiO_2–P_2O_5$) by addition of Li_2O, and Ag^+ ions to the system through applying ion-exchange process to obtain suitable electrical conductivity [1,2] and antibacterial characteristic [11,12]. Afterward, accomplished more investigation of electrical conductivity in this system and modified system with replacing of CaO by Li_2O [3,4]. Effect of ZrO_2 addition on crystallization behavior, porosity and chemical–mechanical properties of a $CaO–TiO_2–P_2O_5$ micro-porous glass ceramic was also investigated [13]. Banijamali et al. improved glass forming ability of $CaO–TiO_2–P_2O_5$ system with Al_2O_3 addition [14].

* Corresponding author at: Department of Materials Engineering, Science and Research Branch, Islamic Azad University, P.O. Box 1478655816, Tehran, Iran. Fax: +98 21 44869784.
E-mail addresses: ahmadi.hamidreza@gmail.com, hr.ahmadi@srbiau.ac.ir (H.R. Ahmadi Mooghari), nemati@sharif.edu (A. Nemati), beftekhari@iust.ac.ir (B. Eftekhari Yekta), zhamnabard@nrcam.org (Z. Hamnabard).

0272-8842/$36.00 © 2011 Elsevier Ltd and Techna Group S.r.l. All rights reserved.
doi:10.1016/j.ceramint.2011.12.034

Structural characterization of the additives in $CaO–TiO_2–P_2O_5$ system has not extensively been studied. Recently, structural characterization of the effect of TiO_2 in $CaO–TiO_2–P_2O_5$ system has investigated by Silva et al. [15] and Lucacel et al. [5]. Gradually increasing of TiO_2 content in the calcium-phosphate glass matrix causes a slow depolymerization of the infinite metaphosphate chains [15]. A progressive depolymerization of the phosphate glass network occurs as TiO_2 content increases but the cohesion of glass structure increases due to the replacing of P–O–P bonds by Ti–O–P bonds [15].

The aim of the present study is to understand the effect of SiO_2 and K_2O in glass structure in the $CaO–TiO_2–P_2O_5$ system.

2. Experimental procedure

The chemical composition of the base glass was $9CaO{\cdot}5TiO_2{\cdot}6P_2O_5$, for which the oxides compositions and samples code are listed in Table 1. The starting materials were reagent grade of $CaCO_3$, TiO_2, H_3PO_4 (85%), SiO_2 and K_2CO_3. After adding water, the mixture was well stirred to make the homogeneous slurry. The slurry was dried at about 110 °C for approximately 16 h. The batches were melted in alumina crucibles at 1450 °C for 1 h under an ambient atmosphere inside of an electric furnace. The melts were poured into a preheated carbon mould. The glass specimens then were annealed at 600 °C for 2 h and allowed to cool down in the furnace.

In order to determine the crystallization temperature and to evaluate crystallization mechanism, differential thermal analysis (DTA) was performed on the glass specimens (Netzsch STA 409 PC Luxx) using samples.

Phase identification of the samples was performed by X-ray diffraction (XRD) analysis using a STOE STADI MP diffractometer with Cu-K_α radiation ($\lambda = 1.54$ Å), operating at 40 kV and 30 mA. The monitoring was carried out in the 2θ range of 10–90°. After polishing and etching, the samples were coated with a thin film of gold and studied with SEM (Vega-Tescan).

The FT-IR spectra of the glasses were obtained in the 400–4000 cm^{-1} spectral range with a spectrometer at room temperature (Thermo Nicolet Nexus 870 FT-IR). The IR spectra measurements were done using the KBr pellet technique.

^{31}P MAS NMR spectra of the glass powders were recorded using a NMR spectrometer (Bruker, Avance 500, operating at 202.4461871 MHz with 45° pulses, spinning rates of 10 kHz, a 45 s recycles delay) and the chemical shift was quoted in ppm from phosphoric acid (85%).

Table 1
Chemical composition of the investigated glasses (weight ratio).

Sample	CaO	TiO_2	P_2O_5	SiO_2	K_2O
S0	28.74	22.75	48.51	0	0
S3	28.74	22.75	48.51	3	0
S6	28.74	22.75	48.51	6	0
S10	28.74	22.75	48.51	10	0
S3K2	28.74	22.75	48.51	3	2
S6K2	28.74	22.75	48.51	6	2
S10K2	28.74	22.75	48.51	10	2
S14K2	28.74	22.75	48.51	14	2

3. Results

The experimental results showed that the base glass (S0 sample) required a rapid quenching; otherwise it would extensively be crystallized. This behavior was related to its limited glass forming ability (GFA).

3.1. DTA analysis

Fig. 1 depicts the DTA thermographs of the glasses with particle range of 0.5–0.6 mm. The DTA results show that GFA

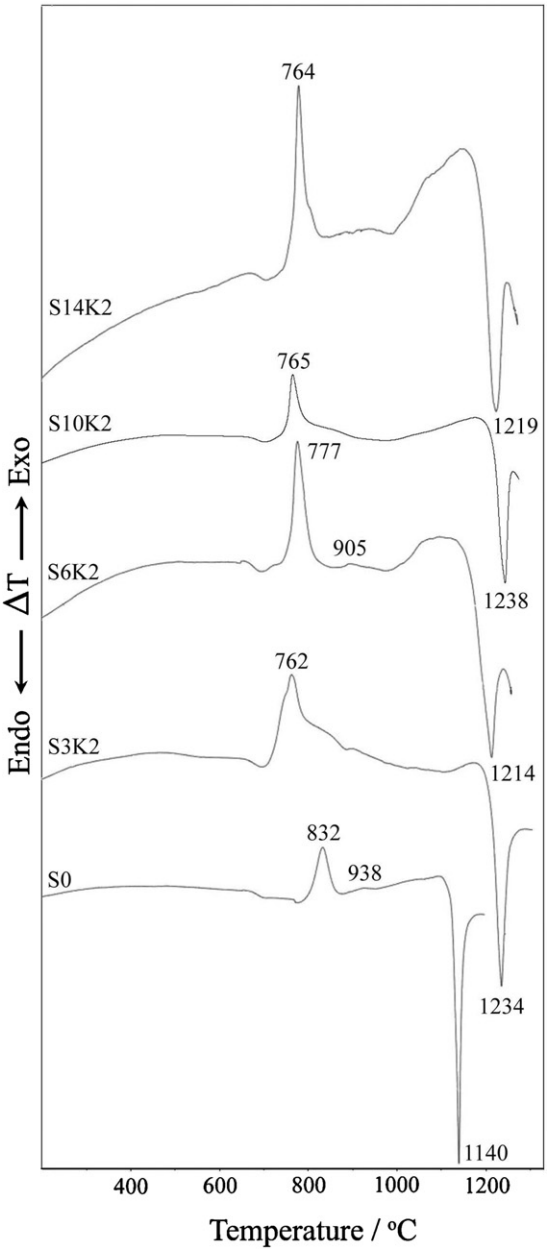

Fig. 1. DTA curves of some investigated glasses.

Table 2
The calculated thermal parameter of samples.

Sample	T_g (°C)	T_X (°C)	T_l (°C)	K_H	$T_{rg} = T_g/T_l$	T_X/T_l	$\Delta T_X = T_X - T_g$ (°C)	$\gamma = T_X/(T_g + T_l)$	$\Delta T_m = (T_l - T_X)$
S0	673	885	1140	0.8313	0.5903	0.7763	212	0.4881	255
S3K2	665	762	1234	0.2055	0.5389	0.6175	97	0.4013	472
S6K2	668	841	1215	0.4625	0.5498	0.6922	173	0.4466	374
S10K2	670	765	1238	0.2008	0.5412	0.6179	95	0.4009	473
S14K2	668	764	1220	0.2105	0.5475	0.6262	96	0.4047	456

of S0 sample is worsened with SiO_2; but it seems that GFA of silica samples improves with the addition of K_2O, whose details will be mentioned later in the XRD analysis.

Furthermore, the glass transition temperature (T_g) remained almost constant; with increasing of SiO_2 content however, the behavior of the last endothermic peak, which shows the liquidus temperature (T_l) of glass in each sample is different. It is obvious that the liquidus temperature has been increased with SiO_2 but its deepness has been decreased; as compared with SiO_2-free specimen. The results showed that S6K2 specimen had the least liquidus temperature and deepness of the all.

There are several parameters regarding glass forming stability on heating. The various thermal parameters which used to evaluate the glass forming ability are shown in Table 2, where ΔT_X, T_g, T_X, T_l, T_{rg}, and K_H are respectively the temperature interval between the glass transition temperature, the crystallization temperature, the liquidus temperature, the reduced glass transition temperature and the Hrubÿ parameter [16,17]. Two crystallization peak temperatures were detected (T_{X1} and T_{X2}) in the DTA profiles of S0 and S3K2 samples. The mean value of them was reported as T_X.

Based on the data presented in Table 2, the parameters T_X/T_l, T_{rg} ($=T_g/T_l$) and γ ($=T_X/(T_g + T_l)$) in different samples showed only a slight change in the measured values, suggesting that the parameters K_H ($=(T_X - T_g)/(T_l - T_X)$), ΔT_X and ΔT_m ($=T_l - T_X$) are more sensitive in the GFA evaluation.

Crystallization mechanism of glasses was determined using DTA profiles of coarse (0.5–0.6 mm) and fine glass particles (<45 μ). Considerable shift in the crystallization peak temperatures was observed in the DTA profiles which are presented in Table 3.

According to Table 3, the temperature difference of the two exothermic peaks of S0 sample is equal to 45 °C, indicates that the surface crystallization has been accrued in the glass.

Table 3
Dependence of peaks crystallization temperature (ΔT) to the particle size of glasses.

Sample	Mesh size	T_X (°C)	T (°C)
SO	325	787	45
	30–35	832	
S3K2	325	736	26
	30–35	762	
S6K2	325	764	13
	30–35	777	
S10K2	325	736	29
	30–35	765	

Besides, the crystallization temperature difference of the two glass particle sizes of SiO_2 and K_2O bearing glass decreases with increasing of SiO_2. It seems that the nucleation behavior of the glasses has changed; and surface devitrification has been modified to bulk devitrification. This trend is more obvious in S6K2 samples.

3.2. XRD analysis

In except of the glass S0, the other glasses were opaque; therefore, in order to confirm the amorphous nature of them, their XRD patterns were analyzed. The XRD results showed that the addition of SiO_2 caused the crystallization of the base glass (S0 sample as shown in Fig. 2). The intensity of peaks rise with the increase of the SiO_2 content; but XRD pattern of the samples with both SiO_2 and K_2O, and annealed at 600 °C, do not exhibit any sharp peaks, which is an indication of amorphous state; as shown in Fig. 3.

3.3. Infrared spectroscopy

FT-IR spectra of glasses in the frequency range between 400 and 4000 cm^{-1} are shown in Fig. 4. All the glasses had similar IR spectra. The largest intensity for the IR lines is at 900–1300 cm^{-1} as shown in Fig. 4. The graph consisted of three peaks corresponding to stretching vibration of P–O–P linkages on Q^1 and Q^2 units, which indicate a large number of pyrophosphate groups and a few metaphosphate groups in the network of these glasses.

The network connectivity is conventionally expressed as Q^n units, where Q and n represent the tetrahedral structural unit

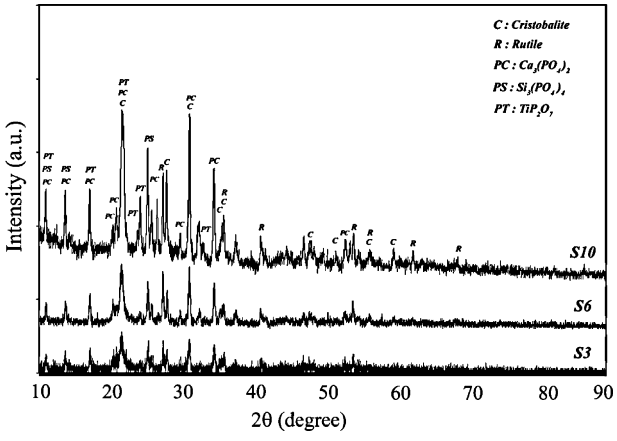

Fig. 2. XRD of annealed S3, S6, S10 samples.

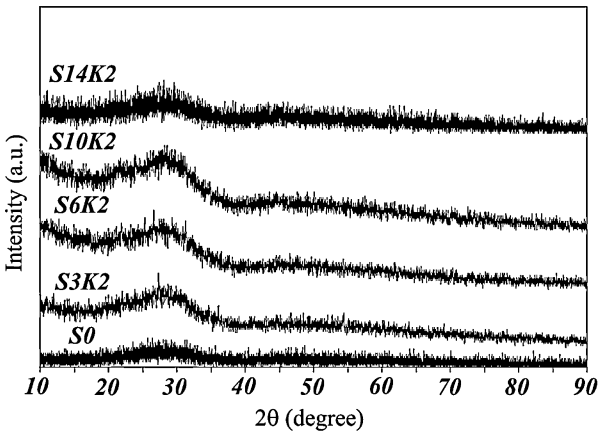

Fig. 3. XRD of annealed S0, S3K2, S6K2, S10K2 samples at 600 °C.

and the number of bridging oxygen per tetrahedron; respectively. For phosphor–oxygen networks, *n* varies between 0 and 3, where, Q^3 presents a pure P_2O_5 structure corresponding to the absence of network modifiers; in which tetrahedra form a cross-linked network. Q^2 forms chains or rings, and Q^1 forms terminal anions, which are intermediate structures, and finally, Q^0 represents forms of isolated anions (PO_4^{3-}). These glasses are defined as ultraphosphates, metaphosphates ($P_2O_6^{2-}$), pyrophosphate ($P_2O_7^{4-}$), and orthophosphates, respectively [18–20].

With adding of SiO_2, two new bands were observed at 500 cm^{-1} and 540 cm^{-1}. The first one can be related to the Si–O–Si bending vibration, which indicates that a silicate network has been formed [21]. The appearance of an incipient Si–O–Si in the FT-IR spectra suggests that silicate groups can be present in a crystal-like environment. The second one may be assigned to frequencies of asymmetric bending vibration of (PO_4^{3-}) [5,19–24]. The only band at 806 cm^{-1} in S10 sample may be attributed to symmetrical bond-stretching vibration of the Si–O–Si [25].

The data indicated that the intensity of the band at 500 cm^{-1} was increased with SiO_2 content (up to 10%). When K_2O was added, it was decreased, but the increase of intensity was again observed with SiO_2 content. The intensity of P–O–P bending bond was also decreased and the band attributing to (PO_4^{3-}) was disappeared. The intensity of O=P–O peak almost becomes extinct with the increase of SiO_2 concentration. The band positions and their assigned chemical bonds are summarized in Table 4.

The observed bands at high frequencies' (1650–1658 cm^{-1}) can be assigned to the different role of H_2O molecule in the structure. It is possible to assume that, the samples absorbed atmospheric moisture or during the preparation of KBr pellets for IR measurements, causing the appearance of IR band of H_2O molecule [26,27].

3.4. ^{31}P MAS NMR

The ^{31}P MAS NMR spectra of samples and the list of the resonance chemical shifts are shown in Fig. 5 and Table 5. In agreement with IR results, the NMR spectra show narrow and

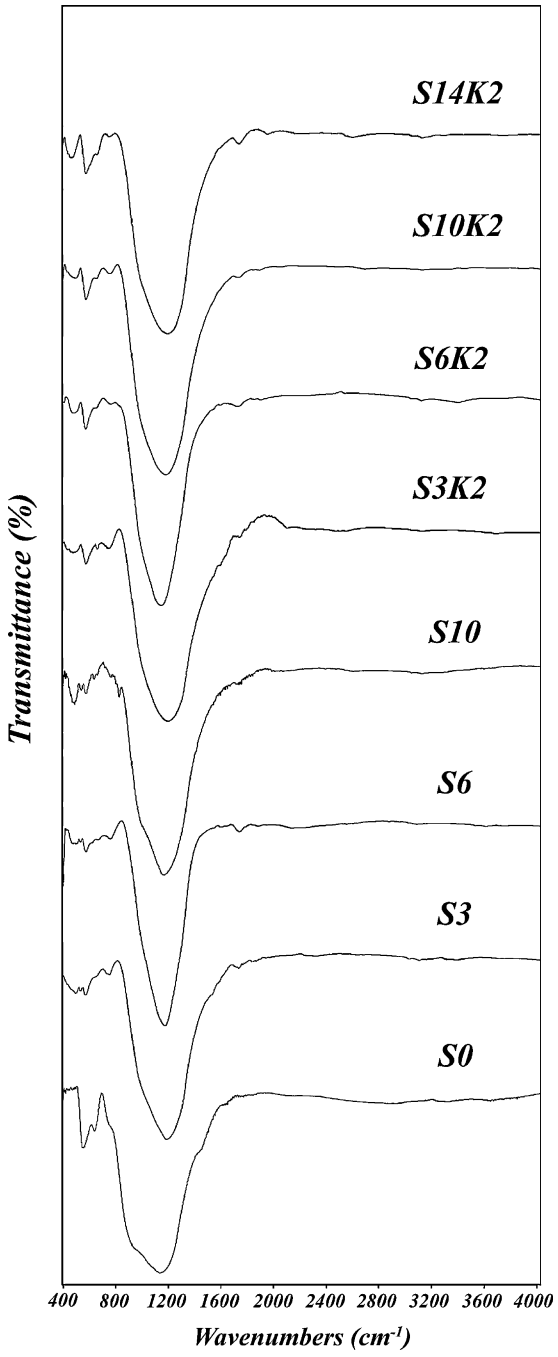

Fig. 4. FT-IR spectra for $CaO–TiO_2–P_2O_5$:$xSiO_2$–2% K_2O glasses.

broad resonance lines of Q^0, Q1 and Q^2 groups. In S0 sample, two resonances can be observed. The broad resonances centered on −12.5 and −33.1 ppm, which are the indication of amorphous environment around the P atoms. The resonance at −12.5 ppm can be assigned to Q^1 units and other can be attributing to Q^2 groups. The mentioned signals indicate that the Q^2 units exist at the base glass but Q^1 units are completely major component in the S0 sample.

Not only, the line width of peaks is changed and become narrower but also Q^1 and Q^2 units are disappeared with the introduction of SiO_2. It seems to us that the appearance of narrow resonances with a chemical shift of 10.2–15.6 ppm and

Table 4
The band positions and their assigned chemical bonds of glasses.

Samples	Band position in cm^{-1}	Chemical bonds	Band position in cm^{-1}	Chemical bonds
S0	566	δ (P–O–P)	937	$\upsilon\ (P–O–P)_{asym}$
	655	O═P–O, P–O–Ti	1140	$\upsilon\ (P–O–P)_{asym}$
	750	$\upsilon\ (P–O–P)_{sym}$	1254	$\upsilon\ (P–O–P)_{asym}$
			1654	H_2O
S3	500	δ (Si–O–Si)	937	$\upsilon\ (P–O–P)_{asym}$
	540	(PO_4^{3-})	950	Si–O–Ti
	566	Ti–O–Si	1140	$\upsilon\ (P–O–P)_{asym}$
	750	TiP_2O_7	1656	H_2O
S6	490	δ (Si–O–Si)	937	$\upsilon\ (P–O–P)_{asym}$
	540	(PO_4^{3-})	950	Si–O–Ti
	566	Ti–O–Si	1140	$\upsilon\ (P–O–P)_{asym}$
	750	TiP_2O_7	1658	H_2O
S10	490	δ (Si–O–Si)	937	$\upsilon\ (P–O–P)_{asym}$
	540	(PO_4^{3-})	950	Si–O–Ti
	566	Ti–O–Si	1120	$\upsilon\ (Si–O–Si)_{asym}$
	630	$\upsilon\ (Ti–O–Ti)_{sym}$	1140	$\upsilon\ (P–O–P)_{asym}$
	750	TiP_2O_7	1654	H_2O
	806	$\upsilon\ (Si–O–Si)_{sym}$		
S3K2	566	Ti–O–Si	937	$\upsilon\ (P–O–P)_{asym}$
	655	P–O–Ti	950	Si–O–Ti
	750	$\upsilon\ (P–O–P)_{sym}$	1140	$\upsilon\ (P–O–P)_{asym}$
			1650	H_2O
S6K2	490	δ (Si–O–Si)	937	$\upsilon\ (P–O–P)_{asym}$
	566	Ti–O–Si	950	Si–O–Ti
	655	P–O–Si	1140	$\upsilon\ (P–O–P)_{asym}$
	750	$\upsilon\ (P–O–P)_{sym}$	1651	H_2O
S10K2	495	δ (Si–O–Si)	937	$\upsilon\ (P–O–P)_{asym}$
	566	Ti–O–Si	950	Si–O–Ti
	655	P–O–Si	1140	$\upsilon\ (P–O–P)_{asym}$
	750	$\upsilon\ (P–O–P)_{sym}$	1657	H_2O
S14K2	470	δ (Si–O–Si)	937	$\upsilon\ (P–O–P)_{asym}$
	566	Ti–O–Si	950	Si–O–Ti
	655	P–O–Si	1140	$\upsilon\ (P–O–P)_{asym}$
	750	$\upsilon\ (P–O–P)_{sym}$	1651	H_2O

with an approximate constant line width can be as an indicative of phosphorus in an orthophosphate environment (PO_4^{3-}). That is in good agreement with previous reports [28,29].

The sharp signals are vanished with adding of K_2O and new broad peaks are appeared at the range of −9.3 to −13.2 ppm, which are assigned to Q^1 units.

Table 5
Position of Q^n species for glass samples.

Sample	Phosphate unit		
	Q^0 (ppm)	Q^1 (ppm)	Q^2 (ppm)
S0	–	−12.5	–33.1
S3	+10.2	–	–
S6	+12.4	–	–
S10	+15.6	–	–
S3K2	–	−9.3	–
S6K2	–	−13.2	–
S10K2	–	−11.5	–
S14K2	–	−10.7	–

3.5. Microstructural evaluation

SEM microphotographs of S3K2 (a), S6K2 (b) and S14K2 (c) samples are presented in Fig. 6. It appears that with the introduction of K_2O to the system phase separation has reduced. K_2O in S3K2 has caused the formation of Ti and P rich regions. EDX patterns presented in Fig. 6 show Si rich droplet regions in the phosphate matrix phase in S6K2 and S14K2 samples.

The peaks intensity of Si and P in EDX pattern of Fig. 6 indicates that with the increase of SiO_2 not only the peak intensity of Si to P is raised but also the numbers of Si and P rich regions are increased.

4. Discussion

4.1. System of TiO_2–CaO–P_2O_5 glass

In the IR spectrum for the base glass (S0), bands are observed at 566, 655, 750, 937, 1140 and 1254 cm^{-1}. The IR

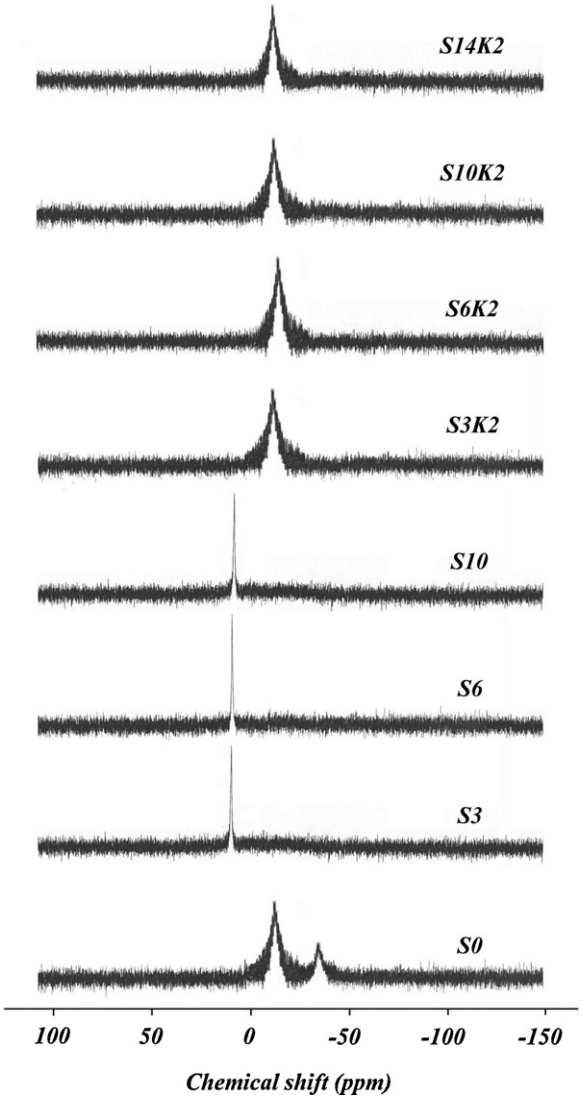

Fig. 5. ^{31}P MAS NMR spectra of the samples.

band at 750 cm^{-1} is attributed to the symmetric of P–O–P bridging oxygen stretching mode vibration bond, in Q^1 units. This is in accordance with the presence of pyrophosphate groups. The pyrophosphate group ($P_2O_7^{4-}$) contains only a single P–O–P linkage and correspondingly exhibits only one band near 700 cm^{-1} [18]. The IR bands at 1254 cm^{-1} is assigned to the asymmetric stretching mode of non-bridging oxygen atoms bonded to phosphorus atoms, the P–O–P, in the phosphate tetrahedra, in Q^2 units. In other words, the 1254 cm^{-1} band is attributed to $(PO_2)_{as}$ units, in the phosphate tetrahedral of the metaphosphate units. Thus, the S0 glass is based on ($P_2O_6^{2-}$) or ($P_2O_7^{4-}$) groups.

The bands at 937 and 1140 cm^{-1} are due to the asymmetric stretching vibration of P–O–P linkages in Q^1 units; these observations are in accordance with other papers [5,18,26,30].

The band at 566 cm^{-1} may be attributed to the deformation modes of phosphate tetrahedral and the vibrations of the cation oxygen polyhedron to form of P–O–P bond bending vibration [22]. The band at 655 cm^{-1} is assigned to bond-bending vibration of O=P–O [21]. The band at 655 cm^{-1} is also attributed to the vibrations of Ti–O bonds in the deformed octahedral or TiO_6 [15,18,23].

In the spectrum of sample S0 (Fig. 4), the band due to TiO_6 structural units seem to be merged with symmetric stretching vibration of P–O–P bond indicating possible linkages of the type P–O–Ti, in the network that observed by several authors [15,18,23]. This is explained by the break of P=O bonds in metaphosphates ($P_2O_6^{2-}$) and the formation of P–O–Ti bonds in pyrophosphate units, which are in accordance with The ^{31}P MAS NMR spectra of S0 sample (Fig. 5).

In agreement with IR results, the ^{31}P MAS NMR spectra of S0 showed only Q^1 and Q^2 groups with broad resonances, which are indicative of amorphous environment around the P atoms. Thus, the ^{31}P MAS NMR and infrared spectrums of the S0 glass show that the pyrophosphate group is the predominant structural unit in this glass.

4.2. Effect of SiO_2 on TiO_2–CaO–P_2O_5 system

In the SiO_2 containing glasses the systematic change in the IR spectra and development of new peaks at low and mid frequency regions, gives more information about the structural change (as shown in Fig. 4).

As shown in Fig. 2, TiP_2O_7 phase is formed in S3, S6 and S10 samples containing SiO_2. The band vibrations of TiO_4 units were found to be active in the IR spectrum in the 770 and 370 cm^{-1}. Krishna et al. have assigned the 740 cm^{-1} band to Ti–O–Ti symmetric stretching vibrations of TiO_4 units [23]. Based on the literature survey [18–23,30], and the vibration of ($P_2O_7^{4-}$) groups in the near 700 cm^{-1} band, it seems reasonable to attribute the band at about 750 cm^{-1} to the common vibrations of TiP_2O_7 structural units in the S3, S6 and S10 samples as detected in the XRD pattern (Fig. 2).

As indicate earlier, besides two new band at 500 cm^{-1} and 540 cm^{-1}, new band was appeared in the mid frequency region at 950 cm^{-1} in SiO_2 containing glasses (Fig. 4). The intensity of this band increases with increasing SiO_2 content. Görlich et al. and Uma et al. have assigned the bands at the 950 cm^{-1} to the possible mode of Si–O–Ti bond. So the band observed at 950 cm^{-1} in S3, S6 and S10 specimens might be due to asymmetrical bond stretching vibrations of the ''dangling ends'' attribute to $Si–O^-$ (the non-bridging oxygen in the [SiO_4] tetrahedra) in the Si–O–Ti bond [25,31]. The band intensity of Si–O–Ti bonding could be considered as a degree of Ti inclusion ions in silica structure.

According to Fig. 4, with increasing of SiO_2 from 6% to 10%, a new weak band appears at 630 cm^{-1} in S10 sample. This band can be ascribed to $Ti–O^-$ (the bridging oxygen between two [TiO_4] tetrahedra) symmetrical bond stretching vibration in Ti–O–Ti. The appearance of this band in the FT-IR spectra may be as an indication of the formation of titanium oxide network (formation of rutile in Fig. 2).

The data indicates that the intensity of 566 cm^{-1} band decrease, with the addition of SiO_2 to the base glass (S0 sample). However, in S3, S6 and S10 specimens, it was increased with silica contents from 3% to 10%. The band at 566 cm^{-1} can be assigned to symmetrical bond stretching

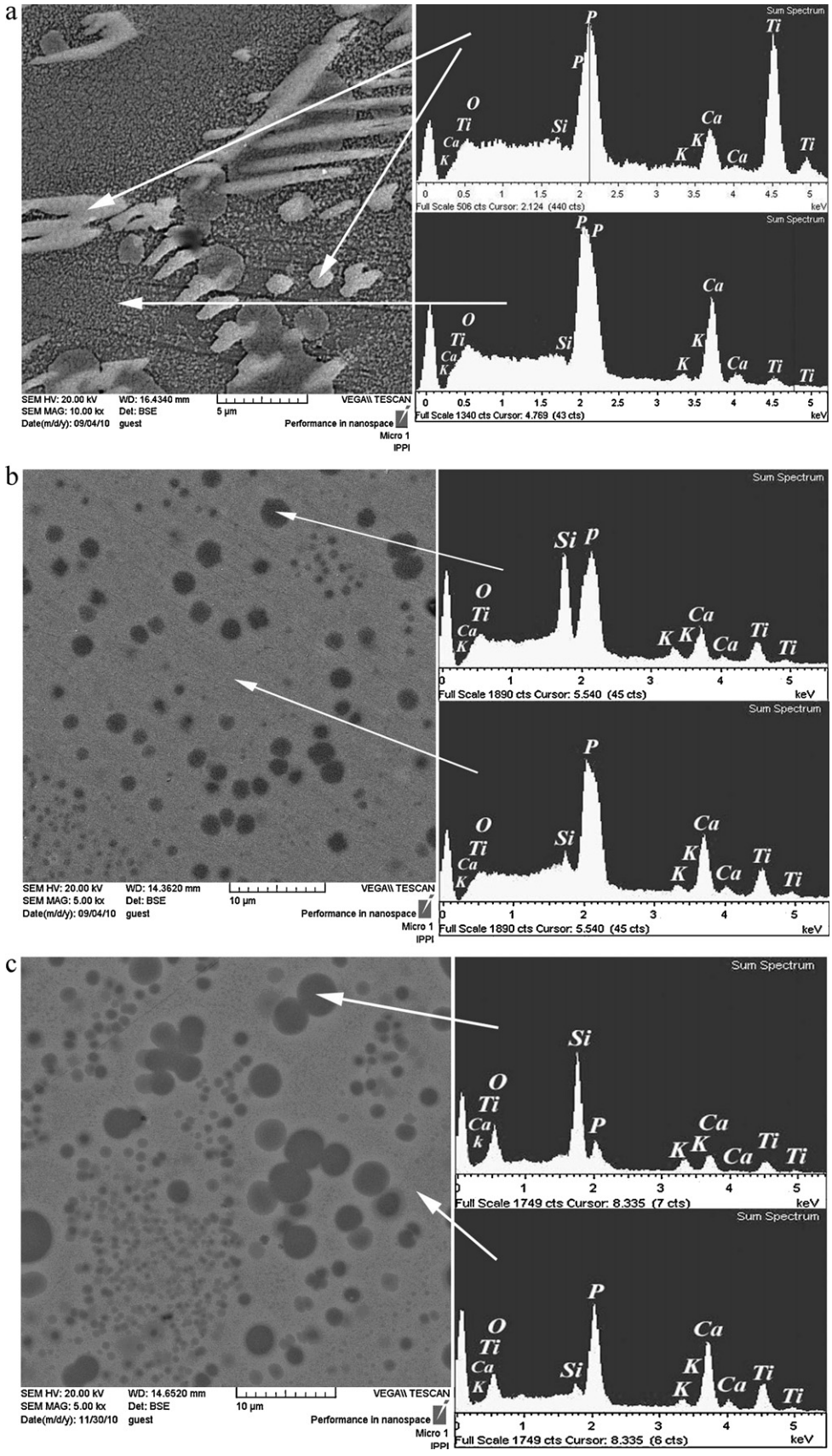

Fig. 6. SEM microphotograph and EDX of S3K2 (a), S6K2 (b) and S14K2 (c) samples.

vibration of the Ti–O^- (the non-bridging oxygen in the [TiO_4] tetrahedra) in Ti–O–Si [25]. The intensity of the band for Ti–O–Si bonding can be considered as a sign of degrees of the inclusion of silicon ions in titanium structure.

Moreover, with the addition of SiO_2, the band of 1254 cm^{-1} in the S0 sample become extinct and a new band appears in the mid frequency region at 1120 cm^{-1} in S10 glass. This might be due to the possible mode of asymmetrical bond stretching vibrations of the Si–O^- (oxygen bridges between the [SiO_4] tetrahedra) in Si–O–Si [25]. It has been reported in the literature that Si–O–Si bond rocking was observed in silicate glasses within 410–490 cm^{-1} range [27]. So the band observed at 470–500 cm^{-1} in SiO_2 containing glasses are due to Si–O–Si bending vibration. This may be as an indication of the formation of a silica network which, in turn, can also be an indication of formation of cristobalite as it has been shown in Fig. 2.

Considering the very strong bond between Si–O and Ti–O, when the glass does not contain a suitable amount of alkali or alkaline earth metal ions (in this research: CaO) as oxygen donors, the Si and Ti will compete in their oxide bonds, and TiO_2 will crystallize in the form of rutile or anatase [32]. Görlich et al. [25] has also shown that the solution of TiO_2 in SiO_2 is not easily the task, so that glassy solutions can be obtained in a metastable state. Under these conditions and probably the difference of field strength between both oxides, phase separation takes place in the system [25,32]. One phase contains tetrahedral ([SiO_4] as well as [TiO_4]); but rich in SiO_2, the other one contains the octahedra ([TiO_6] as well as a small proportion of [SiO_6]), especially in large quantities of TiO_2 which finally crystallizes as rutile [25]. Li et al. [33] and Linati et al. [34] stated that in the SiO_2–P_2O_5 glasses, when the amount of P_2O_5 is high, SiO_2 and P_2O_5 cannot form complete solutions in the system. Thus based on the literature survey, it seems reasonable to assume that the Ti–O–Ti and Si–O–Si bonds in the FT-IR spectra may be as an indication of the formation of a titanium oxide and silica networks as rutile and cristobalite; respectively, which are in accordance with XRD pattern (Fig. 2). These observations are more sensible in the greater amount of SiO_2 (such as S10 specimen). Moreover, as SiO_2 is added a new band at 540 cm^{-1} is appeared to attributing to (PO_4^{3-}) units. The appearance of (PO_4^{3-}) units may be relevant to phosphorous in a crystal-like environment [19].

In agreement with IR results, the ^{31}P MAS NMR spectra of samples containing SiO_2 (Fig. 5) showed the sharp signals that can be as an indicative of phosphorus in an orthophosphate environment (PO_4^{3-}). The sharp and narrow signals indicate the appearance of new crystalline phases [35]. Thus considering XRD pattern (Fig. 2), the formation of (PO_4^{3-}) units may be implying the formation of crystalline phase(s) such as $Si_3(PO_4)_4$ and $Ca_3(PO_4)_2$ phases.

4.3. Effect of SiO_2 along with K_2O on system of TiO_2–CaO–P_2O_5 glass

Since Fig. 3 shows no sharp peaks it can be considered as an amorphous state, which might be the effect of addition of K_2O as a modifier.

It seems that with adding of SiO_2 the bond of P–O–Ti at 655 cm^{-1} becomes extinct but the addition of K_2O in the S6K2, S10K2 and S14K2 glasses lead to the displacement of P–O–Ti with more covalence in nature bond of P–O–Si. In a similar study, Ahsan et al. [27] observed the band at 650 cm^{-1} can be ascribed to P–O–Si asymmetric bending vibration of SiO_6 octahedra rather than Si–O–Si tetrahedral. Higher the amount of silica, higher the peak intensity, particularly at 470–490 cm^{-1} ranges that is attributed to bending vibration of Si–O–Si. This may be as an indication of the formation of a silica network, especially in the greater amount of silica (such as S14K2). But it seems that K_2O in S3K2 has caused the formation of Ti and P rich regions. The data indicates that in the sample containing 3% SiO_2 Si and P rich regions were not formed; which showed that probably, the P–O–Si bond does not form in the system. So, the weak band of 655 cm^{-1} attributes to the P–O–Ti bond.

As it was expected, K_2O promoted the formation of glass and suppressed the tendency for separation into immiscible phases. A similar result has been reported in soda-potash glasses [32]. Moreover, Morimoto [36] showed that K_2O suppresses the crystallization in the Li_2O–SiO_2 glass. Thus in accordance with Fig. 3, K_2O prevents crystallization of glasses. Therefore, TiP_2O_7 phase does not form with the introduction of K_2O. Consequently, the band vibration at 750 cm^{-1} is attributed to the symmetric of P–O–P bridging oxygen stretching mode vibration bond, in Q^1 units, in accordance with the ^{31}P MAS NMR spectra. The bands at 630 cm^{-1} ascribing to Ti–O–Ti, 806 cm^{-1} and 1120 cm^{-1} assigning to Si–O–Si are also vanished. This may be an indication of the tendency for less formation of titanium and silica structures.

Li et al. [33] has shown that in Na_2O–SiO_2–P_2O_5 glasses, SiO_2 and P_2O_5 form a silica–phosphate network, when the content of Na_2O is lower than P_2O_5. Meanwhile, Iwamoto and Tsunawaki [37] stated that the role of K^+ ion in SiO_2 is the same as that of Na^+ ion. Note that K_2O and Na_2O have almost similar properties. It could be said that, when the content of K_2O is lower than P_2O_5, SiO_2 and P_2O_5 form a silica–phosphate network (as P–O–Si bond), probably with the replacement of P^{5+} site by Si^{4+} via the breakdown of phosphate network. These results can be used to confirm the formation of isolated droplet phases separated from phosphate matrix phase that are rich of Si and P (as shown in Fig. 6).

The peak intensity of Si and P in EDX pattern of Fig. 6 shows that with the increase of SiO_2, the peak intensity of Si to P, and the number of Si and P rich regions has increased. This may be an indication that these areas are away from the structure of phosphate–silica and are close to the silicate structure. Furthermore, the intensity of 566 cm^{-1} band rises with increasing of SiO_2. According to Fig. 6, it seems that this bond attributing to 566 cm^{-1} band throughout the matrix. As mentioned earlier, Görlich et al. [25] revealed that the TiO_2 in SiO_2 is not easily solved. Therefore it is not expected to increase the number of Ti–O–Si bond throughout the matrix with the raising of SiO_2. So it is possible to assume that with the increase of SiO_2, Si is removed from the titanium structure and forms the Si richer regions of isolated droplet shape.

As presented in section of DTA analysis, according to Fig. 1 the liquidus temperature has been increased with SiO_2 and its deepness has been decreased with SiO_2; in comparison with SiO_2-free specimen. S6K2 specimen has the least liquidus temperature and deepness of the all. The decreasing of liquidus temperature is compatible with the Rawson glass-forming theory, which predicts that decreasing of liquidus temperature leads to the better glass-forming ability [38].

The data in Table 2 clearly indicates that GFA in S0 sample has been worsened with the increase of SiO_2; but it seems that S6K2 sample showed the best GFA of all except S0.

As in Fig. 4, the weak shoulder at 950 cm^{-1} is relevant to the bond of Si–O–Ti. Another bond of Ti–O–Si is observed at 566 cm^{-1}. Based on these two bonds, it can be assumed that silica structure includes less content of titanium ions.

Based on the data presented in Fig. 4, there are the bands of asymmetric stretching vibration of P–O–P linkages at 937 and 1140 cm^{-1} and asymmetric stretching vibration of P–O–P at 750 cm^{-1} in Q^1 units, as well as the band at 1254 cm^{-1} assigning to the asymmetric stretching mode of P–O–P in the phosphate tetrahedra, in Q^2 units disappears. ^{31}P MAS NMR spectrum of glasses in Fig. 5, show that with adding of K_2O, the sharp signals are vanished, and the new broad peaks are formed, assign to Q^1 units. These are not sufficiently sharp peaks to be related to crystalline phases and can be as a sign of the amorphous environment around the P atoms.

Thus, considering the above description, it can be stated that despite addition of SiO_2 along with K_2O, the ^{31}P MAS NMR and infrared spectrums of glasses show no Q^2 sites in the phosphate network and the formation of Q^1 and the pyrophosphate group is the predominant structural unit in these glasses.

5. Conclusions

The structure of $CaO–TiO_2–P_2O_5$ glass changed with the introduction of SiO_2. With the adding of SiO_2, TiP_2O_7 phase is formed in S3, S6 and S10. Furthermore, the appearance of Ti–O–Ti and Si–O–Si bonds in the FT-IR spectra may be as an indication of the formation of a titanium oxide and silica networks as rutile and cristobalite respectively.

K_2O prevents crystallization of glasses and promotes the formation of glass. The addition of K_2O in the S6K2, S10K2 and S14K2 glasses lead to deletion of the TiP_2O_7, rutile, cristobalite and the displacement of P–O–Ti by more covalent P–O–Si. In the greater amount of silica (S14K2) form the bending vibration of Si–O–Si bond. K_2O in S3K2 has caused the formation of Ti and P rich regions. It appears that 3% SiO_2 could not cause the formation of Si and P rich regions. Furthermore, K_2O caused the formation of phosphate–silica network as P–O–Si, and formation of isolated droplet phases separated from phosphate matrix phase that are rich of Si and P. The best and optimum condition for silicon ions in phosphate structure is to act as a glass former, as obtained in S6K2 glass. S6K2 specimen has the least liquidus temperature and deepness of the all. The decreasing of liquidus temperature is compatible with the Rawson glass-forming theory to the better glass-forming ability that well-matched with GFA parameters.

With the introduction of K_2O, the surface devitrification has been trepanned to bulk devitrification especially in S6K2 samples.

Despite addition of SiO_2 together with K_2O the ^{31}P MAS NMR and infrared spectrums of glasses show that no Q^2 sites will remain in the phosphate network and the formation of Q^1 and the pyrophosphate group is the predominant structural unit in these glasses.

References

[1] H. Hosono, Y. Abe, Fast lithium conducting glass–ceramics in the CaO–Li_2O–TiO_2–Al_2O_3–P_2O_5 system, Solid State Ionics 44 (1991) 293–297.

[2] H. Hosono, Y. Abe, Porous glass–ceramics with a skeleton of the fast-lithium-conducting crystal $Li_{1+x}Ti_{2-x}Al_x(PO_4)_3$, Journal of the American Ceramic Society 75 (10) (1992) 2862–2864.

[3] B.K. Money, K. Hariharan, Lithium ion conduction in lithium metaphosphate based systems, Applied Physics A 88 (2007) 647–652.

[4] X. Xu, Z. Wen, X. Yang, J. Zhang, Z. Gu, High lithium ion conductivity glass–ceramics in Li_2O–Al_2O_3–TiO_2–P_2O_5 from nanoscaled glassy powders by mechanical milling, Solid State Ionics 177 (2006) 2611–2615.

[5] R.C. Lucacel, M. Maier, V. Simon, Structural and in vitro characterization of TiO_2–CaO–P_2O_5 bioglasses, Journal of Non-Crystalline Solids 356 (2010) 2869–2874.

[6] T.Y. Wei, Y. Hu, L.G. Hwa, Structure and elastic properties of low-temperature sealing phosphate glasses, Journal of Non-Crystalline Solids 288 (1–3) (2001) 140–147.

[7] Y. Daiko, H. Yajima, T. Kasuga, Preparation of porous titanium phosphate glass–ceramics for NH3 gas adsorption with self-cleaning ability, Journal of the European Ceramic Society 28 (2008) 267–270.

[8] S.V. Dorozhkin, Amorphous calcium (ortho)phosphates, Acta Biomaterialia 6 (2010) 4457–4475.

[9] A. Kishioka, Glass formation in the Li_2O- TiO_2- P_2O_5, MgO- TiO_2- P_2O_5 and CaO- TiO_2- P_2O_5 systems, *Bulltin of the Chemical Society of Japan* 51 (9) (1978) 2559–2561.

[10] H. Hosono, Z. Zhang, Y. Abe, Porous glass–ceramics in the CaO–TiO_2–P_2O_5 systems, Journal of the American Ceramic Society 71 (1989) 587–1590.

[11] H. Hosono, Y. Abe, Silver ion selective porous lithium titanium phosphate glass–ceramics cation exchanger and its application to bacteriostatic materials, Materials Research Bulletin 29 (1994) 1157–1162.

[12] T. Kasuga, H. Kume, Y. Abe, Porous glass–ceramic with bacteriostatic properties in silver-containing titanium phosphates: control of release of silver ions from glass–ceramics into aqueous solution, Journal of the American Ceramic Society 80 (1997) 777–780.

[13] M. Kord, V.K. Marghussian, B. Eftekhari-yekta, A. Bahrami, Effect of ZrO_2 addition on crystallization behaviour, porosity and chemical–mechanical properties of a CaO–TiO_2–P_2O_5 micro-porous glass ceramic, Materials Research Bulletin 44 (2009) 1670–1675.

[14] S. Banijamali, A.R. Aghaei, B. Eftekhari Yekta, Improving glass-forming ability and crystallization behavior of porous glass–ceramics in CaO–Al_2O_3–TiO_2–P_2O_5 system, Journal of Non-Crystalline Solids 356 (2010) 1569–1575.

[15] A.M.B. Silva, R.N. Correia, J.M.M. Oliveira, M.H.V. Fernandes, Structural characterization of TiO_2–P_2O_5–CaO glasses by spectroscopy, Journal of the European Ceramic Society 30 (2010) 1253–1258.

[16] M.L.F. Nascimento, L.A. Souza, E.B. Ferreira, E.D. Zanotto, Can glass stability parameters infer glass forming ability? Journal of Non-Crystalline Solids 351 (2005) 3296–3308.

[17] C.T. Rios, S. Suriñach, M.D. Baró, C. Bolfarini, W.J. Botta, C.S. Kiminami, Glass forming ability of the Al–Ce–Ni system, Journal of Non-Crystalline Solids 354 (2008) 4874–4877.

[18] A. Shaim, M. Et-tabirou, Role of titanium in sodium titanophosphate glasses and a model of structural units, Materials Chemistry and Physics 80 (2003) 63–67.

[19] H. Aguiar, E.L. Solla, J. Serra, P. González, B. León, N. Almeida, S. Cachinho, E.J.C. Davim R.Correia, J.M. Oliveira, M.H.V. Fernandes,

Orthophosphate nanostructures in SiO_2–P_2O_5–CaO–Na_2O–MgO bioactive glasses, Journal of Non-Crystalline Solids 354 (2008) 4075–4080.
[20] D. Carta, J.C. Knowles, M.E. Smith, R.J. Newport, Synthesis and structural characterization of P_2O_5–CaO–Na_2O sol–gel materials, Journal of Non-Crystalline Solids 353 (2007) 1141–1149.
[21] N. Shibata, M. Horigudhi, T. Edahiro, Raman spectra of binary high-silica glasses and fibers containing GeO_2, P_2O_5 and B_2O_3, Journal of Non-Crystalline Solids 45 (1981) 115–126.
[22] S.T. Reis, M. Karabulut, D.E. Day, Chemical durability and structure of zinc–iron phosphate glasses, Journal of Non-Crystalline Solids 292 (2001) 150–157.
[23] G.M. Krishna, N. Veeraiah, N. Venkatramaiah, R. Venkatesan, Induced crystallization and physical properties of Li_2O–CaF_2–P_2O_5:TiO_2 glass system. Part I. Characterization, spectroscopic and elastic properties, Journal of Alloys and Compounds 450 (2008) 477–485.
[24] C. Ivascu, A.T. Gabor, O. Cozar, L. Daraban, I. Ardelean, FT-IR, Raman and thermoluminescence investigation of P_2O_5–BaO–Li_2O glass system, Journal of Molecular Structure 993 (2011) 249–253.
[25] E. Görlich, K. Blaszczak, A. Stoch, G. Siemiiiska, The devitrification of glasses in the binary system SiO_2–TiO_2, Materials Chemistry 5 (1980) 289–302.
[26] Y.M. Lai, X.F. Liang, S.Y. Yang, J.X. Wanga, L.H. Cao, B. Dai, Raman and FTIR spectra of iron phosphate glasses containing cerium, Journal of Molecular Structure 992 (2011) 84–88.
[27] M.R. Ahsan, M.G. Mortuza, Infrared spectra of xCaO$(1 - x - z)$$SiO_2$$z$$P_2O_5$ glasses, Journal of Non-crystalline Solids 351 (2005) 2333–2340.
[28] M.D. O'Donnell, S.J. Watts, R.V. Law, R.G. Hill, Effect of P_2O_5 content in two series of soda lime phosphosilicate glasses on structure and properties – Part I: NMR, Journal of Non-Crystalline Solids 354 (2008) 3554–3560.
[29] R.K. Brow, Review: the structure of simple phosphate glasses, Journal of Non-Crystalline Solids 263–264 (2000) 1–28.
[30] E.A.A. Neel, W. Chrzanowski, S.P. Valappil, L.A. O'Dell, D.M. Pickup, M.E. Smith, R.J. Newport, J.C. Knowles, Doping of a high calcium oxide metaphosphate glass with titanium dioxide, Journal of Non-Crystalline Solids 355 (2009) 991–1000.
[31] T. Uma, M. Nogami, Influence of TiO_2 on proton conductivity in fuel cell electrolytes based on sol–gel derived P_2O_5–SiO_2 glasses, Journal of Non-Crystalline Solids 351 (2005) 3325–3333.
[32] M.B. Volf, Chemical Approach to Glass, Elsevier Science Publishing Company Inc., 1984.
[33] D. Li, M.E. Fleet, G.M. Bancroft, M. Kasrai, Y. Pan, Local structure of Si and P in SiO_2–P_2O_5 and Na_2O–SiO_2–P_2O_5 glasses: a XANES study, Journal of Non-Crystalline Solids 188 (1995) 181–189.
[34] L. Linati, G. Lusvardi, G. Malavasi, L. Menabue, M.C. Menziani, P. Mustarelli, A. Pedone, U. Segre, Medium-range order in phosphosilicate bioactive glasses: insights from MAS-NMR spectra, chemical durability experiments and molecular dynamics simulations, Journal of Non-Crystalline Solids 354 (2008) 84–89.
[35] H.-L. Ren, Y. Yue, C.-H. Ye, L.-P. Guo, J.-H. Lei, NMR study of crystallization in MgO–CaO–SiO_2–P_2O_5 glass–ceramics, Chemical Physics Letters 292 (1998) 317–322.
[36] S. Morimoto, Effect of K_2O on crystallization of Li_2O–SiO_2 glass, Journal of the Ceramic Society of Japan 114 (2006) 195–198.
[37] N. Iwamoto, Y. Tsunawaki, Raman spectra of K_2O–SiO_2 and K_2O–SiO_2–TiO_2 glasses, Journal of Non-Crystalline Solids 18 (1975) 303–306.
[38] H. Rawson, Proc. IV Intern Congress on Glass Impremenic Chaix, Paris, (1956), p. 62.